Applied Physics Letters

Magnetotransport in a strain superlattice of graphene

Cite as: Appl. Phys. Lett. **115**, 143508 (2019); https://doi.org/10.1063/1.5125462
Submitted: 23 August 2019 . Accepted: 18 September 2019 . Published Online: 02 October 2019

Yingjie Zhang, Youngseok Kim, Matthew J. Gilbert, and Nadya Mason

Applied Physics Letters ARTICLE scitation.org/journal/apl

Magnetotransport in a strain superlattice of graphene

Cite as: Appl. Phys. Lett. **115**, 143508 (2019); doi: 10.1063/1.5125462
Submitted: 23 August 2019 · Accepted: 18 September 2019 ·
Published Online: 2 October 2019

Yingjie Zhang,[1,2,a)] Youngseok Kim,[3] Matthew J. Gilbert,[3,4] and Nadya Mason[2,5]

AFFILIATIONS

[1]Department of Materials Science and Engineering, University of Illinois, Urbana, Illinois 61801, USA
[2]Frederick Seitz Materials Research Laboratory, University of Illinois, Urbana, Illinois 61801, USA
[3]Department of Electrical and Computer Engineering, University of Illinois, Urbana, Illinois 61801, USA
[4]Department of Electrical Engineering, Stanford University, Stanford, California 94305, USA
[5]Department of Physics, University of Illinois, Urbana, Illinois 61801, USA

[a)]Author to whom correspondence should be addressed: yjz@illinois.edu

ABSTRACT

Three-dimensional (3D) deformation of two-dimensional materials offers a route toward band structure engineering. In the case of graphene, a spatially nonuniform deformation and strain are known to generate an effective magnetic field, i.e., a pseudomagnetic field, although experimental realization of this effect in electronic devices has been challenging. Here, we engineer the 3D deformation profile of graphene to create a strain superlattice and study the resultant magnetotransport behavior both experimentally and via quantum transport simulations. We observe a weakening of superlattice features as we increase the magnetic field, which we find to be consistent with competing interactions between the external magnetic field and the strain-induced pseudomagnetic field. Our results demonstrate that strain superlattices are promising platforms to modulate the band structure and engineer the electronic transport behavior in graphene.

Graphene, a two-dimensional (2D) hexagonal lattice of carbon atoms, allows versatile engineering of electronic phases at the atomically thin device scaling limit. While intrinsic graphene exhibits massless Dirac fermion states,[1,2] in the presence of mechanical deformation, graphene's band structure can change significantly.[3–14] Theoretically, a two-dimensional strain field $u_{ij}(x,y)$ in graphene gives rise to a gauge field $\boldsymbol{A} = \frac{\beta}{a}\begin{pmatrix} u_{xx}-u_{yy} \\ -2u_{xy} \end{pmatrix}$, where a and β are constants related to the lattice length and hopping parameter, respectively.[3,4] This gauge field produces a pseudomagnetic field $B^{ps} = \frac{\partial A_y}{\partial x} - \frac{\partial A_x}{\partial y}$, which modulates graphene's band structure in the same way as an external magnetic field, except that B^{ps} has opposite signs at the two valleys K and K'.[4] Since B^{ps} is determined by the spatial gradients of the strain tensor $u_{ij}(x,y)$, a nonzero B^{ps} requires a spatially nonuniform strain. Carefully designed spatial profiles of B^{ps} are predicted to exhibit various mesoscopic effects ranging from zero-field quantum Hall states to topological insulating phases.[4–8] However, in realistic experimental systems demonstrated so far, such as graphene nanobubbles, ridges, and drumheads, there is limited control of the spatial distribution of B^{ps}.[9–11] Oftentimes the strain and B^{ps} are strongly localized, resulting in a localized wave function.[6,11] While the presence of B^{ps} has been observed via local probe measurements,[9–11] due to the random nanoscale fluctuations, the effect of B^{ps} on electronic transport in a mesoscopic system has been elusive.

To understand the impact of nonuniform strain on device-level behavior, we fabricated a system where strain varies periodically across the whole graphene channel. The periodic strain variation generates additional Dirac points, i.e., superlattice Dirac points (SDPs), in the band structure of graphene, which can be observed by electronic transport measurements.[15] This strain superlattice was achieved by depositing graphene on an array of SiO_2 nanospheres (NSs), where graphene experiences a periodic strain variation with a magnitude up to ~2%.[16] We previously confirmed superlattice transport under no external magnetic field.[15] Here, we study the magnetotransport behavior of this system to probe the possible effects of a pseudomagnetic field.

The device schematic is shown in Fig. 1(a), where the NS diameter is ~20 nm, the SiO_2 film (300 nm thick)/Si substrate serves as the gate dielectric and back gate, and Au serves as the top contact for graphene. The NSs form a nearly periodic hexagonal close-packed pattern, as shown in the scanning electron microscopy image [Fig. 1(b)]. The device geometry and Dirac point positions are summarized in Table I. For the given NS size, the SDPs are expected to occur at

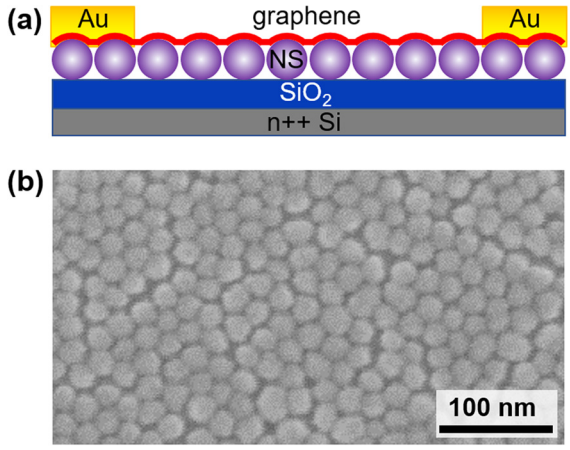

FIG. 1. (a) Schematics of the graphene strain superlattice device, which consists of 2-terminal Au contacts, graphene, SiO_2 nanospheres (~20 nm diameter), SiO_2 dielectric (300 nm thick), and n++ Si as the back gate. (b) Scanning electron microscopy (SEM) image of the SiO_2 nanosphere assembly.

$n = \pm 4n_0$ ($\pm 1 \times 10^{12}$ cm^{-2}),[17–21] where $n_0 = 2.5 \times 10^{11}$ cm^{-2} corresponds to 1 electron per superlattice unit cell. This factor of four comes from the fourfold degeneracy in the valley and spin degrees of freedom in graphene. At the SDPs, the density of states is nearly zero, and the conductance is expected to drop below the normal value. The predicted conductance dips at the SDPs, with a strain-dependent magnitude, has been previously observed in these strain superlattice devices.[15]

It has also been shown that different graphene-on-NS devices exhibit different strain magnitudes.[15] This device-to-device variation is likely induced by the device fabrication processes which can lead to a partial strain release. For the current study, we use two superlattice devices having different strains, together with a control device—flat, unstrained graphene on a SiO_2/Si substrate (with the same 2-terminal Au contacts). The two graphene-on-NS devices are marked "low-strain" and "high-strain" (Table I), corresponding to devices having smaller and larger superlattice conductance dips (at zero external magnetic field), respectively.[15] The magnetotransport data of these three devices are shown in Figs. 2(a)–2(c). For each device, we measure the conductance (G) as a function of the gate voltage (V_G) and magnetic field (B), convert the gate voltage to carrier density (n), and plot dG/dn as a function of n and B.[15] These 2D plots are typically referred to as the Landau fan diagrams. In these plots [Figs. 2(a)–2(c)], the blue regions, with $dG/dn \sim 0$, correspond to either conductance plateaus or conductance dips. All the measurements are performed at 2 K.

TABLE I. Channel length (L) and width (W) of all the devices.

Device	Experimental, control[b]	Experimental, low-strain[c]	Experimental, high-strain[c]	Simulation
L (μm)	1.65	1.8	2.2	0.248
W (μm)	1.8	1.5	1.6	0.212
Dirac point (V)[a]	9.6	23.0	13.7	0

[a]The Dirac point is defined as the gate voltage at which the conductance is minimum.
[b]The control device consists of unstrained graphene on the flat SiO_2 substrate.
[c]The strain magnitudes in the graphene-on-NS devices are qualitatively compared using the magnitudes of the superlattice conductance dips (at zero external magnetic field).

For the control device [Fig. 2(a)], we observe the standard half-integer quantum Hall effect of graphene,[1,2] with plateaus occurring at filling factors $\nu = n\phi_0/B = \pm 2, \pm 6, \pm 10, \ldots$ (labeled by black arrows), where ϕ_0 is the flux quantum. The Landau fans of each plateau can be linearly traced to the main Dirac point (DP). In the low-strain superlattice device [Fig. 2(b)], plateaus show up at the same filling factors as those of the control device when $B > 4$ T (black lines and arrows). However, at lower fields, new conductance dip features emerge from superlattice Dirac points (SDPs) at $n = \pm 4n_0$ ($\pm 1 \times 10^{12}$ cm^{-2}) (red lines and arrows). At $n = -4n_0$, the Landau fans follow superlattice filling factors $\nu_s = -2$; while at $n = 4n_0$, there is a fan feature with $\nu_s = 2$. The assignment of the exact filling factor numbers may not be fully accurate at this low-field range, due to the broad width of the conductance dip features (originating from the disorder in the NS packing structure), but the trend in evolution of the Landau fans with the magnetic field is clear. For the high strain device [Fig. 2(c)], besides the plateaus with filling factors $\nu = \pm 2$ originating from the main DP (black lines and arrows), there are fan structures with $\nu_s = \pm 2$ emerging from the SDP at $n = -4n_0$ (red lines and arrows). These conductance dip/plateau features extend to the maximum measured field $B = 9$ T at both sides of the SDP, in contrast to the weak strain device where the superlattice fans disappear around 4 T.

The weakening of superlattice features under a finite magnetic field has not been experimentally observed before in graphene superlattice systems. In fact, the previously studied graphene/boron nitride superlattice systems show pronounced superlattice features under a magnetic field as high as 45 T,[21] corresponding to a Landau gap of about 240 meV. This is much higher than the superlattice modulation amplitude, estimated to be only 10–50 meV for graphene/boron nitride.[19,20] The reason why the electrostatic superlattice effect is observed at a high external magnetic field is because the periodic on-site electrostatic potential modulation is independent of the external field.

Unlike the graphene/boron nitride system, we estimated that the magnitude of electrostatic potential and charge doping in our superlattices is too small (less than random doping fluctuations) to induce any observable superlattice effects.[15] We thus expect that the susceptibility of superlattice modulation to the magnetic field in our system is related to strain-induced effects, which need to be treated in the framework of the pseudomagnetic field. The pseudomagnetic field arises due to the modulation in the hopping constants between neighboring sites in the tight-binding picture. Due to this modulation, the charge carrier acquires a modified phase as it travels from one site to the other, similar to the Peierls substitution under an external magnetic field. As a result, the effective local magnetic field is given as $B_{eff}(\boldsymbol{r}) = B + B^{ps}(\boldsymbol{r})$, where B is the applied external field and $B^{ps}(\boldsymbol{r})$ is the inhomogeneous pseudomagnetic field induced by the strain. Under zero or a low magnetic field, the band structure is modified by the periodically placed localized disorders. When such periodicity is strong enough to induce a superlattice miniband, we will observe the secondary Dirac points. In the presence of a large external magnetic field, the system should be analyzed in the framework of the quantum Hall effect in the presence of disorders, which broaden or add fine structures in incompressible regions. Therefore, the secondary Dirac point may not be

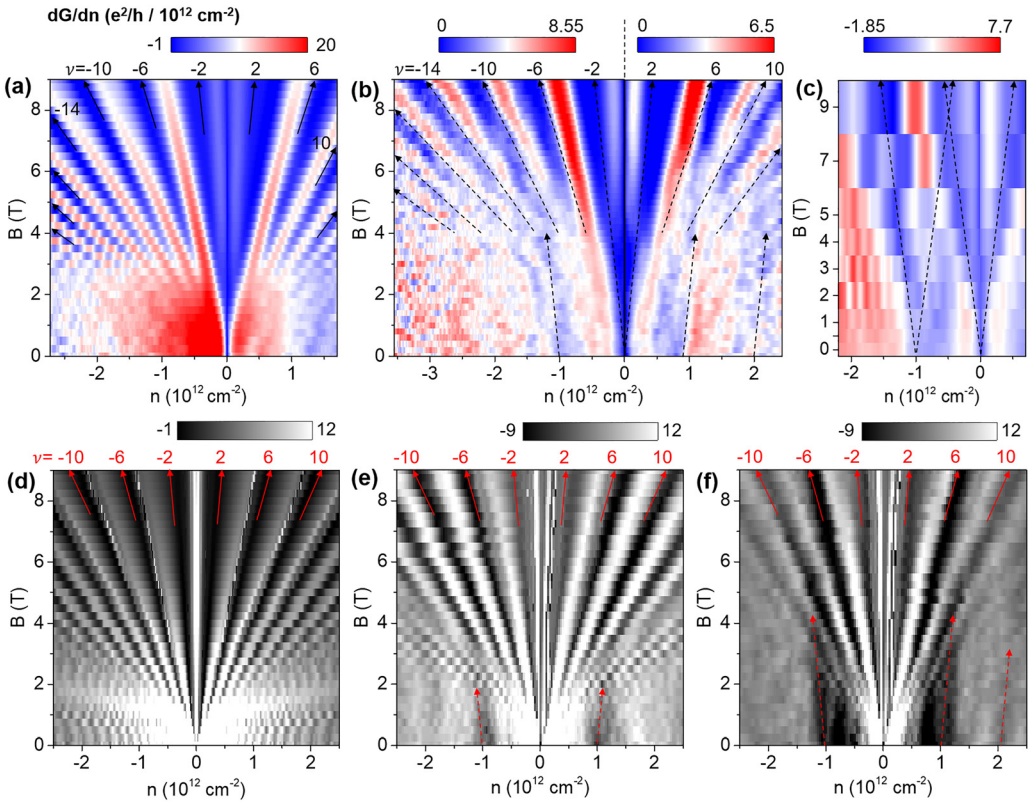

FIG. 2. Experimental (a)–(c) and simulated (d)–(f) magnetotransport results. The experimental results are shown as 2D plots of d*G*/d*n* as a function of carrier density (*n*) and magnetic field (*B*) for a control device of flat, unstrained graphene (a), a low strain superlattice device (b), and a high strain superlattice device (c). At $n < 0$, the sign of d*G*/d*n* is reversed so that larger values represent higher absolute slopes in the *G* vs *n* curve. The solid and dashed lines/arrows mark the Landau fans emerging from the main DPs and SDPs ($n \approx \pm 4n_0, \pm 8n_0$, where $n_0 = 2.5 \times 10^{-11}$ cm^{-2}), respectively. The scale of dG/dn is normalized by the same factor in the three plots (a)–(c), where zero corresponds to conductance plateaus with no slope change. The measured carrier density range is limited by the mechanical stability of the devices under large gate voltages, likely due to the presence of suspended parts of graphene between adjacent NSs. (d)–(f) are the simulated 2D plots of d*G*/d*n* for a control system with no strain (d), a low-strain system (e), and a high strain system (f). Similar to the experimental results, the conductance dip/plateau features originating from the main DPs and SDPs are marked by lines/arrows.

observed once the magnetic field is strong enough to drive the system into the quantum Hall regime. The crossover between the superlattice effect and quantum Hall effect may occur near the point where the external field is close to the average magnitude of the pseudomagnetic field.

To quantitatively analyze the possible role of strain in the magnetotransport features, we perform quantum transport simulations using a tight-binding model. We write the Hamiltonian of graphene as:[15]

$$H = \sum_n \sum_{\alpha=1,2,3} [t_\alpha(\boldsymbol{r}_n) e^{i\varphi_{\alpha,n}} c_A^\dagger(\boldsymbol{r}_n) c_B(\boldsymbol{r}_n + \boldsymbol{\delta}_\alpha) + h.c.] + \sum_n V(\boldsymbol{r}_n)[c_A^\dagger(\boldsymbol{r}_n) c_A(\boldsymbol{r}_n) + c_B^\dagger(\boldsymbol{r}_n + \boldsymbol{\delta}_1) c_B(\boldsymbol{r}_n + \boldsymbol{\delta}_1)], \quad (1)$$

where $c_A(\boldsymbol{r}_n)$ and $c_B(\boldsymbol{r}_n)$ are the electron annihilation operators at site $\boldsymbol{r}_n = (x_n, y_n)$ of the sublattice A and B, respectively, at the nth unit cell. $V(\boldsymbol{r}_n)$ is the on-site potential at position $\boldsymbol{r}_n$. $\alpha = 1, 2, 3$ corresponds to the nearest neighbor, hopping from the A to B sublattice in three different directions. These nearest neighbor vectors can be written as

$$\boldsymbol{\delta}_1/a = (0, 1), \quad \boldsymbol{\delta}_2/a = \left(-\sqrt{3}/2, -1/2\right), \quad \boldsymbol{\delta}_3/a = \left(\sqrt{3}/2, -1/2\right), \quad (2)$$

where a is the lattice constant of graphene. $t_\alpha(\boldsymbol{r}_n)$ is the hopping constant at position $\boldsymbol{r}_n$ in the direction $\boldsymbol{\delta}_\alpha$. In the presence of an external magnetic field (B), the Peierl's substitution introduces the phase term in the Hamiltonian:[22]

$$\varphi_{\alpha,n} = \frac{e}{h} \int_{\boldsymbol{r}_n}^{\boldsymbol{r}_n + \boldsymbol{\delta}_\alpha} \boldsymbol{A} \cdot d\boldsymbol{l}. \quad (3)$$

Here, we use the vector potential $\boldsymbol{A} = -By\hat{x}$. In the case of graphene, the phase factors become

$$\varphi_{1,n} = 0, \quad \varphi_{2,n} = -\varphi_{3,n} = \frac{2\pi}{3} \frac{B\mathcal{A}_0}{\Phi_0} \left(\frac{y_n}{a} + \frac{1}{4}\right), \quad (4)$$

where $\mathcal{A}_0 = 3\sqrt{3}a^2/2$ is the area of the unit cell and $\Phi_0 = h/e$ is the flux quantum.

In the presence of strain and lattice distortion, the hopping parameter (t) changes to

$$t + \delta t = t \exp\left(-\beta\left(a'/a - 1\right)\right), \quad (5)$$

where a' and a are the bond length of the strained and unstrained graphene, respectively, and $\beta = 3.37$.[23]

We use the experimentally imaged NS profile [Fig. 1(b)] to construct the superlattice deformation pattern of graphene, and then formulate the Hamiltonian using Eq. (1). We simulate the conductance using the nonequilibrium Green's function (NEGF) method.[24] The simulated magnetotransport results are shown in Figs. 2(d)–2(f). The simulated control device, an intrinsic, unstrained graphene, shows the standard half-integer quantum Hall effect that is commonly observed in graphene[1,2] [Fig. 2(d)], which is very similar to the corresponding experimental data shown in Fig. 2(a). In the presence of spatial strain variations in graphene, with a magnitude of ∼1.9% and ∼6.8%, the simulated results are shown in Figs. 2(e) and 2(f). In both systems, superlattice conductance dips at $n = \pm 4n_0$ develop at $B = 0$ T. In the low strain system [Fig. 2(e)], this dip feature extends up to ∼2 T (with filling factors $\nu_s = -2$ or 2). In the high strain system [Fig. 2(f)], this feature goes up to ∼4 T ($\nu_s = -2$ or 2); at higher fields, Landau fans follow the same pattern as normal, uniform graphene. This behavior is qualitatively consistent with the experimentally observed features in Figs. 2(b) and 2(c), and confirms that superlattice effects can survive up to higher magnetic fields when the system is more strongly strained. Note that the simulated results are not completely identical to the experimental data in terms of the range of magnetic field where superlattice Landau fan features exist. One possible reason is that the experimental deformation profile of graphene deviates from the simplified Gaussian height profile used in the simulations.[15] It is likely that the strain in graphene shows large spikes on top of the nanospheres, which result in a stronger pseudomagnetic field effect than the simulated system with smooth Gaussian variations.

Since the superlattice magnetotransport is sensitive to strain modulation, both experimentally and in the simulations, we expect the pseudomagnetic field to play a role in magnetotransport. An external magnetic field (B) leads to spatially uniform Landau quantization and a global energy gap, while the strain modulation results in a spatially varying pseudomagnetic field (B^{ps}) and local energy gap.[4] As shown in Fig. 3, if the pseudomagnetic field dominates ($B^{ps} \gg B$), superlattice effects will prevail; if the external magnetic field is much higher than the pseudomagnetic field ($B^{ps} \ll B$), however, the system will have a nearly spatially uniform Landau gap and exhibit the standard quantum Hall effect of normal graphene. When the external magnetic field is of similar magnitude to the pseudomagnetic field ($B^{ps} \sim B$), we expect the electrons to be partially localized at local spots with the maximum B^{ps}, and partially localized at the edge (induced by the external field). As the external field becomes larger, there can be a transition for the electrons to be fully edge-localized, which induces a change in the transport feature (from superlattice transport to the quantum Hall effect).

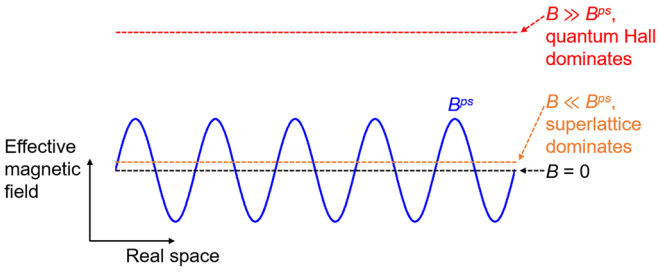

FIG. 3. Schematic diagram showing the interaction of the pseudomagnetic field (B^{ps}) with the real magnetic field (B) in a strain superlattice of graphene. When $B \ll B^{ps}$, the superlattice effect dominates; when $B \gg B^{ps}$, the quantum Hall effect dominates and superlattice behaviors will be smeared out.

In the above analysis, we assumed that the real and pseudomagnetic fields can be directly added, for each valley state of graphene. This can be derived from the tight-binding model of graphene, as shown in the supplementary material.

In summary, we have studied the magnetotransport behaviors of a strain superlattice of graphene. We observed a transition from superlattice transport to the quantum Hall effect as the external magnetic field increases, likely due to the competition between the real and pseudomagnetic field. Precise engineering of strain and pseudomagnetic field patterns in graphene can enable a variety of low-dissipation electronics and valleytronics device applications.[4–8]

See the supplementary material for the magnetotransport curves and derivation of the additivity of real and pseudomagnetic fields.

Y.Z. acknowledges support from the University of Illinois at Urbana-Champaign. N.M., Y.K., and M.J.G. acknowledges support from the NSF-MRSEC under Award No. DMR-1720633. M.J.G. acknowledges support from the National Science Foundation under Grant No. ECCS-1351871. This work was carried out in part in the Frederick Seitz Materials Research Laboratory Central Facilities and in the Beckman Institute at the University of Illinois.

REFERENCES

[1]K. S. Novoselov, A. K. Geim, S. V. Morozov, D. Jiang, M. I. Katsnelson, I. V. Grigorieva, S. V. Dubonos, and A. A. Firsov, Nature **438**, 197 (2005).
[2]Y. Zhang, Y.-W. Tan, H. L. Stormer, and P. Kim, Nature **438**, 201 (2005).
[3]J. L. Mañes, Phys. Rev. B **76**, 045430 (2007).
[4]F. Guinea, M. I. Katsnelson, and A. K. Geim, Nat. Phys. **6**, 30 (2010).
[5]T. Low and F. Guinea, Nano Lett. **10**, 3551 (2010).
[6]M. Settnes, S. R. Power, M. Brandbyge, and A.-P. Jauho, Phys. Rev. Lett. **117**, 276801 (2016).
[7]X.-P. Zhang, C. Huang, and M. A. Cazalilla, 2D Mater. **4**, 024007 (2017).
[8]P. Ghaemi, J. Cayssol, D. N. Sheng, and A. Vishwanath, Phys. Rev. Lett. **108**, 266801 (2012).
[9]N. Levy, S. A. Burke, K. L. Meaker, M. Panlasigui, A. Zettl, F. Guinea, A. H. Castro Neto, and M. F. Crommie, Science **329**, 544 (2010).
[10]H. Yan, Y. Sun, L. He, J.-C. Nie, and M. H. W. Chan, Phys. Rev. B **85**, 035422 (2012).
[11]N. N. Klimov, S. Jung, S. Zhu, T. Li, C. A. Wright, S. D. Solares, D. B. Newell, N. B. Zhitenev, and J. A. Stroscio, Science **336**, 1557 (2012).
[12]A. Reserbat-Plantey, D. Kalita, Z. Han, L. Ferlazzo, S. Autier-Laurent, K. Komatsu, C. Li, R. Weil, A. Ralko, L. Marty, S. Gueron, N. Bendiab, H. Bouchiat, and V. Bouchiat, Nano Lett. **14**, 5044 (2014).
[13]S. T. Gill, J. H. Hinnefeld, S. Zhu, W. J. Swanson, T. Li, and N. Mason, ACS Nano **9**, 5799 (2015).
[14]J. H. Hinnefeld, S. T. Gill, and N. Mason, Appl. Phys. Lett. **112**, 173504 (2018).
[15]Y. Zhang, Y. Kim, M. J. Gilbert, and N. Mason, npj 2D Mater. Appl. **2**, 31 (2018).
[16]Y. Zhang, M. Heiranian, B. Janicek, Z. Budrikis, S. Zapperi, P. Y. Huang, H. T. Johnson, N. R. Aluru, J. W. Lyding, and N. Mason, Nano Lett. **18**, 2098 (2018).
[17]C. H. Park, L. Yang, Y. W. Son, M. L. Cohen, and S. G. Louie, Phys. Rev. Lett. **101**, 126804 (2008).
[18]M. Yankowitz, J. Xue, D. Cormode, J. D. Sanchez-Yamagishi, K. Watanabe, T. Taniguchi, P. Jarillo-Herrero, P. Jacquod, and B. J. LeRoy, Nat. Phys. **8**, 382 (2012).

[19]L. A. Ponomarenko, R. V. Gorbachev, G. L. Yu, D. C. Elias, R. Jalil, A. A. Patel, A. Mishchenko, A. S. Mayorov, C. R. Woods, J. R. Wallbank, M. Mucha-Kruczynski, B. A. Piot, M. Potemski, I. V. Grigorieva, K. S. Novoselov, F. Guinea, V. I. Fal'ko, and A. K. Geim, Nature **497**, 594 (2013).
[20]C. R. Dean, L. Wang, P. Maher, C. Forsythe, F. Ghahari, Y. Gao, J. Katoch, M. Ishigami, P. Moon, M. Koshino, T. Taniguchi, K. Watanabe, K. L. Shepard, J. Hone, and P. Kim, Nature **497**, 598 (2013).
[21]B. Hunt, J. D. Sanchez-Yamagishi, A. F. Young, M. Yankowitz, B. J. LeRoy, K. Watanabe, T. Taniguchi, P. Moon, M. Koshino, P. Jarillo-Herrero, and R. C. Ashoori, Science **340**, 1427 (2013).
[22]J. M. Luttinger, Phys. Rev. **84**, 814 (1951).
[23]V. M. Pereira, A. H. Castro Neto, and N. M. R. Peres, Phys. Rev. B **80**, 045401 (2009).
[24]S. Datta, *Quantum Transport: Atom to Transistor* (Cambridge University Press, New York, 2005).